HIV-1 Vif disrupts phosphatase feedback regulation at the kinetochore, leading to a pronounced pseudo-metaphase arrest

Dhaval A. Ghone[1, 2, 6], Edward L. Evans III[1, 3, 5, 6, 7], Madison Bandini[1, 3, 5], Kaelyn G. Stephenson[1], Nathan M. Sherer[1, 4, 5, *], Aussie Suzuki[1, 4, *]

1. McArdle Laboratory for Cancer Research, Department of Oncology, University of Wisconsin-Madison, Madison, Wisconsin, USA
2. Biophysics Graduate Program, University of Wisconsin-Madison, Madison, Wisconsin, USA
3. Cancer Biology Graduate Program, University of Wisconsin-Madison, Madison, Wisconsin, USA
4. Carbone Comprehensive Cancer Center, University of Wisconsin-Madison, Madison, Wisconsin, USA
5. Institute for Molecular Virology, University of Wisconsin-Madison, Madison, Wisconsin 53706, USA
6. These authors contributed equally
7. Present address: Laboratory for Optical and Computational Instrumentation, University of Wisconsin-Madison, Madison, Wisconsin, 53705, USA

* Corresponding authors: Aussie Suzuki (aussie.suzuki@wisc.edu) and Nathan Sherer (nsherer@wisc.edu)

Abstract

The human immunodeficiency virus type 1 (HIV-1) Virion Infectivity Factor (Vif) targets and degrades cellular APOBEC3 proteins, key regulators of intrinsic and innate antiretroviral immune responses, thereby facilitating HIV-1 infection. While Vif's role in degrading APOBEC3G is well-studied, Vif is also known to cause cell cycle arrest but the detailed nature of Vif's effects on the cell cycle has yet to be delineated. In this study, we employed high-temporal single-cell live imaging and super-resolution microscopy to monitor individual cells during Vif-induced cell cycle arrest. Our findings reveal that Vif does not affect the G2/M boundary as previously thought. Instead, Vif triggers a unique and robust pseudo-metaphase arrest, which is markedly distinct from the mild prometaphase arrest induced by the HIV-1 accessory protein, Vpr, known for modulating the cell cycle. During Vif-mediated arrest, chromosomes align properly to form a metaphase plate but later disassemble, resulting in polar chromosomes. Notably, unlike Vpr, Vif significantly reduces the levels of both Phosphatase 1 (PP1) and 2 (PP2) at kinetochores, which are key regulators of chromosome-microtubule interactions. These results reveal a novel function of Vif in kinetochore regulation that governs the spatial organization of chromosomes during mitosis.

Introduction

The human immunodeficiency virus type 1 (HIV-1) weakens the immune system by killing CD4+ T cells, eventually causing the acquired immunodeficiency syndrome (AIDS) (Deeks et al, 2015; Swanstrom & Coffin, 2012). Consequently, individuals infected with HIV-1 have an increased susceptibility to specific cancers and other health complications (Cohen et al, 2016; Grulich et al, 2007; Hernández-Ramírez et al, 2017; Parkin, 2006). After HIV-1 enters a host cell, its RNA genome undergoes reverse transcription to form double-stranded DNA, followed by integration of the DNA provirus into the host's genome. Using the host's transcriptional machinery, HIV-1 transcribes its genome into spliced, partially spliced and completely unspliced viral mRNAs, facilitating viral gene expression and infectious virion production (Jouvenet et al, 2009; Nguyen & Hildreth, 2000; Ono & Freed, 2001).

HIV-1 encodes four accessory viral proteins (Vif, Vpr, Vpu, and Nef) that can be nonessential for virus replication in some ex vivo cell culture systems (Gabuzda et al, 1992) but play crucial immunomodulatory roles in vivo (Malim & Emerman, 2008). The primary role of Vif (Virion Infectivity Factor) is to facilitate the proteasomal degradation of certain members of the APOBEC3 (A3) family of cytidine deaminases (e.g., A3F, A3G, and A3H). In the absence of Vif, A3 proteins associate with HIV-1 genome during the incorporation into assembling virus particles. During the subsequent round of infection, A3 proteins introduce deleterious mutations

into the HIV-1 genome by deaminating cytosine residues in the viral single-stranded DNA during reverse-transcription, converting them to uracil (Chiu & Greene, 2009; Okada & Iwatani, 2016). Vif orchestrates A3 protein degradation by recruiting an E3 ubiquitin ligase complex (Conticello et al, 2003; Marin et al, 2003; Sheehy et al, 2003; Stopak et al, 2003; Yu et al, 2003). This degradation prevents A3 proteins from being incorporated into budding viral particles, ensuring that the progeny virions remain infectious.

Independently of its primary role of A3 protein degradation (DeHart et al, 2008; Du et al, 2019; Zhao et al, 2015), several studies have shown Vif to induce cell cycle arrest and cell death in CD4+ T cells and several other cell types (DeHart et al., 2008; Du et al., 2019; Greenwood et al, 2016; Marelli et al, 2020; Nagata et al, 2020; Sakai et al, 2006; Salamango et al, 2019; Zhao et al., 2015). However, the molecular mechanisms that underpin these effects remain unclear. An earlier study suggested that p53, a major tumor suppressor protein, is required for Vif-induced G2/M cell cycle arrest (Izumi et al, 2010). Other studies demonstrated that Vif can lead to reductions in Cyclin F (Augustine et al, 2017), a non-canonical cyclin critical for late S- and G2-phase progression (Clijsters et al, 2019; Enrico et al, 2021), or affect both Cdk1 and Cyclin B1, which are essential for the transition into and out of mitosis (Sakai et al, 2011). More recently, several studies have shown that Vif's cell cycle arrest activity correlates with the loss of B56 proteins, which are regulatory subunits of protein phosphatase 2A (PP2A)

(DeHart et al., 2008; Du et al., 2019; Greenwood et al., 2016; Marelli et al., 2020; Nagata et al., 2020; Salamango et al., 2019; Salamango et al, 2020; Zhao et al., 2015). The PP2A-B56 complex is known to play a critical role in various key processes during G2 and mitotic processes (Lee et al, 2017; Schuhmacher et al, 2019).

These prior studies predominantly employed flow cytometry-based techniques to measure cell cycle phase population densities. However, an important limitation of flow cytometry is its inability to distinguish between late S, G2, and M phases, as it categorizes cell cycle phases solely based on relative DNA content. Therefore, in this study, we prioritized the use of high-temporal single-cell live imaging techniques that allow us to directly observe disruptions in the cell cycle triggered by Vif expression. We demonstrate that Vif induces a highly unique and robust pseudo-metaphase arrest, irrespective of cell line tested or p53 status, which is distinct from the effects of Vpr, also well-known to affect the cell cycle. Vif disrupts the recruitment of PP2A-B56 to kinetochores during prometaphase, causing a slight yet significant delay in the alignment of chromosome at metaphase. This disruption results in reduced localization of the Astrin-SKAP-PP1 complex at the kinetochores, leading to improper kinetochore-microtubule binding affinity due to increased phosphorylation of the microtubule binding protein at kinetochores. These effects create unbalanced forces between sister chromatids, resulting in misaligned chromosomes and abnormal chromosomal movements.

These insights provide a deeper understanding of Vif's impact on the regulation of the host cell cycle, a conserved feature of Vif that may have potential relevance to HIV-1 pathogenesis in vivo.

Results

Vif and Vpr induce distinct forms of mitotic arrest

Previous research demonstrated that both Vif and Vpr expression causes cell cycle arrest and cytotoxicity in CD4+ T cells and as well as many cancer cell lines (Augustine *et al.*, 2017; Emerman, 1996; Evans *et al*, 2018; Nagata *et al.*, 2020; Sakai *et al.*, 2011; Sakai *et al.*, 2006; Salamango *et al.*, 2019; Salamango *et al.*, 2020; Wang *et al*, 2011; Wang *et al*, 2008). To study the nature of the cell cycle arrest induced by Vif, we first employed high-temporal live cell imaging of a Cal51 reporter cell line engineered for reliable tracking of the cell cycle through endogenous tagging of Histone H2B with mScarlet to monitor chromosomal DNA and Tubulin with mNeonGreen to monitor the microtubule cytoskeleton (Scribano et al, 2021) (**Fig 1A**). Cal51 cells were ideal for this long-term live cell imaging assay due to their adherent nature allowing for long-term single cell monitoring and exhibiting a stable karyotype (Lynch et al, 2022). For these experiments, we infected cells with HIV-1 reporter viruses expressing either Vif ("Vif"), Vpr ("Vpr"), a combination of both ("Vif+Vpr"), or a lack of both ("Control") (**Fig S1A**). These reporter viruses express cyan fluorescent protein (CFP) from the viral *nef* locus, allowing us to identify infected cells using fluorescence microscopy. To focus our study on the effects of these proteins on the cell cycle, the CFP reporter viruses were also engineered to not express

the viral Env and Nef proteins, which can exhibit cytotoxicity (Elder, 2002; Emerman, 1996; Evans *et al.*, 2018).

We assessed the mitotic duration, defined as the time between nuclear envelope breakdown (NEBD) and anaphase onset, in infected (CFP-positive) cells using video microscopy. Vif-expressing Cal51 cells demonstrated a prolonged mitosis lasting ~16 hours, compared to only 30 min in Control cells (**Fig 1B, S1B, and Movies S1-2**). The majority of Vif-expressing cells eventually succumbed to apoptotic cell death or exhibited mitotic slippage, where the cell exited mitosis without completing chromosome segregation (**Fig 1C**).

Vpr has been known to induce G2/M arrest in a variety of cell types, based on data from flow cytometric analysis (Bartz *et al*, 1996; Elder, 2002; Emerman, 1996; Hall *et al*, 2024; He *et al*, 1995; Jowett *et al*, 1995; Sakai *et al.*, 2006). Accordingly, we next compared the differences in G2/M arrests induced by Vif and Vpr. Our high temporal resolution live-cell imaging revealed that Vpr-expressing cells experienced a prolonged mitosis of ~2 hours, which was significantly shorter than the duration observed in Vif-expressing cells (**Fig 1A-B**). Interestingly, Vif+Vpr co-expressing cells exhibited a prolonged mitosis lasting ~22 hours, indicating that Vif plays a dominant role in promoting mitotic arrest when both proteins are present. Supporting this, the majority of Vif-expressing or Vif+Vpr co-expressing mitotic cells underwent apoptotic cell death, whereas Vpr-expressing mitotic cells often completed division or experienced mitotic slippage

(**Fig 1C**). In summary, although both Vif and Vpr can induce a prolonged mitosis, Vif's induction of metaphase arrest is significantly more severe and more likely to lead to cell death.

Unique features of Vif-induced pseudo-metaphase arrest

To pinpoint the specific sub-stage of mitosis affected by Vif expression, we closely assessed chromosome alignment during metaphase. Notably, most Vif-expressing Cal51 cells successfully achieved metaphase chromosome alignment (metaphase plate) similar to Control cells but with a slight delay, reaching alignment approximately 1.5 hours post-NEBD compared to the control's ~30 minutes (**Fig 2A-C and Movies S1-2**). However, this alignment was unstable and deteriorated over time in Vif-expressing cells.

Mitotic arrest induced by common mitotic inhibitors is typically observed in prometaphase before the cells achieve the metaphase plate (Choi et al, 2011). However, the mitotic arrest caused by Vif was distinctive because cells were able to complete prometaphase but then gradually lost proper chromosome spatial organization at the metaphase plate over time. Accordingly, we termed this block "pseudo-metaphase arrest". Consistent with our findings in Cal51 cells, other commonly used cell lines for cell cycle studies, such as HeLa and MDA-MB-231, also demonstrated significant mitotic arrest (approximately 12 hours for both) following Vif expression, which subsequently led to either apoptotic cell death or mitotic

slippage (**Fig S1C-E and S2A-C**). Similar to Cal51, the majority of Vif-expressing cells in these lines were able to establish a metaphase plate early but were unable to enter anaphase (**Fig S1F-G and S2D-E**). Consistent with these results, Vif-expressing HeLa cells exhibited a markedly higher mitotic index compared to Control cells at 72 hours post-infection in fixed immunofluorescence (IF) (**Fig S1H**). In conclusion, Vif triggers a marked pseudo-metaphase arrest in a range of cell lines. Most of these arrested cells experienced either apoptotic cell death or mitotic slippage, suggesting a conserved underlying mechanism.

To confirm that Vif expression alone is sufficient to induce a robust pseudo-metaphase arrest in the absence of other viral factors, we engineered HeLa cells to conditionally express Vif from a codon-optimized mRNA (CO-Vif) under the control of a doxycycline-inducible promoter (Das et al, 2016). Codon-optimization ensured Vif expression in the absence of the HIV-1 Rev protein, which is required to activate Vif expression in the context of the intact viral genome (Behrens & Sherer, 2023). As a control, we employed the same system but with mNeonGreen expression instead of Vif. Control cells displayed mNeonGreen signals approximately 10 hours post-doxycycline induction. In line with these expression kinetics, cells expressing CO-Vif almost invariably exhibited pseudo-metaphase arrest roughly 10 hours post-induction. These cells remained arrested for ~15h, in contrast to Control cells that completed mitosis in ~1 hour (**Fig 2D-E**). While Control cells continued to propagate, cells

expressing Vif did not, confirming that Vif expression alone is sufficient to trigger prolonged pseudo-metaphase arrest and subsequent apoptotic cell death (**Fig 2F-G**).

Vif accelerates G2 progression with no effect on the G1 or S phases

We next asked if Vif altered other stages of the cell cycle in addition to mitosis. To this end, we developed a novel method that allowed us to accurately distinguish between G1, S, and G2 phases in individual Cal51 reporter cells during live cell imaging based on tracking changes to the intensity of Histone H2B-mScarlet over time (see **Methods**). This method offered the advantage of allowing us to measure temporal changes of the DNA content at single cell resolution with high accuracy. Briefly, during S phase, H2B-mScarlet signals increased steadily, eventually plateauing and remaining constant throughout the G2 phase. **Fig 3A** presents example images and an intensity profile covering the period from the end of one mitosis to the beginning of the next in a Control Cal51 cell. Using this method, we observed no significant differences in the durations of either G1 or S phases in both Control or Vif-expressing cells. However, Vif-expressing cells exhibited a slight yet statistically significant reduction in G2 phase duration compared to Control cells (**Fig 3B-C and S3A**). Consistent to Cal51 cells, Vif expression also did not significantly impact the duration of interphase in two additional cell lines, RPE1 and MDA-MB-231 cells (**Fig S3B).** In summary, these findings demonstrated that Vif

expression induces pseudo-metaphase arrest without notably affecting the overall duration of interphase (the cumulative time of G1, S, and G2 phases).

Vif induces pseudo-metaphase arrest independently of p53

A previous study indicated that Vif-induced cell cycle arrest is due to tumor suppressor p53 (Izumi et al., 2010), which is well known for triggering G2 cell cycle arrest in response to DNA damage (St Clair et al, 2004; Stark & Taylor, 2006; Taylor & Stark, 2001). Given that we had already observed Vif inducing pseudo-metaphase arrest in cell lines with functionally inactivated p53, such as HeLa (Evans et al., 2018; Wang et al., 2011) and MDA-MB-231 (Olivier et al, 2002) (**Fig S1C-D and S2A-B**), we further investigated the potential p53-dependency by assessing Vif's effects in p53 null knockout (p53 KO) RPE1 (Mardin et al, 2015) or HCT116 cell lines (**Fig 3D-G**). Both wild-type (p53 +/+) and p53 KO RPE1 and HCT116 cells demonstrated significant pseudo-metaphase arrest in response to viral Vif expression. Specifically, RPE1 wild-type cells were arrested for >10 hours, RPE1 p53 KO cells for ~25 hours, and both HCT116 wild-type and p53 KO cells for >6 hours. In contrast, cells infected with the Vif-negative Control virus showed no delay in mitosis (~30 min for both cell lines) (**Fig 3D-E and S3D-E**). All tested cell lines, regardless of p53 status, arrested in metaphase in the presence of Vif expression (**Fig 3F-G and S3F-G**), with most Vif-expressing cells ultimately exhibiting apoptotic

cell death or mitotic slippage (**Fig S3C and S3H**).

Vif-induced pseudo-metaphase arrest disrupts spatial organization of chromosomes and spindle poles

To further characterize the mitotic defects caused by Vif expression, we next carefully assessed Vif's effects on chromosome alignment at the metaphase plate. To this end, we employed super-resolution microscopy and stained for CENP-C, microtubules, and DNA (see **Methods**). CENP-C is a marker for kinetochores that form the platforms for microtubule attachment on mitotic chromosomes. Our findings revealed that ~100% of Vif-expressing mitotic cells exhibited misaligned chromosomes, with the great majority of these misaligned chromosomes concentrated at spindle poles as polar chromosomes (**Fig 4A-B and S4A**).

We next explored the dynamics of chromosome spatial organization in Vif-expressing cells by using live cell imaging. To do this, we first quantified the proportion of cells exhibiting polar chromosomes at any time point during metaphase/pseudo-metaphase for all four of our cell systems (HeLa, RPE1, MDA-MB-231, and Cal51 cells). Consistent with our fixed-cell analysis, we observed ~100% of Vif-expressing cells exhibiting misaligned polar chromosomes at some time point during the prolonged mitosis, in contrast to Control cells, in which misaligned chromosomes were only rarely observed (**Fig S4B**). To define the dynamic nature of

chromosome movements, we segmented cells into two compartments, polar and equatorial, and then measured the Histone H2B-mScarlet signals within each of these compartments in Cal51 cells over time (**Fig 4C**). Vif-expressing cells exhibited an initial decrease in the frequency of polar chromosomes shortly after NEBD, but this frequency increased significantly during the extended pseudo-metaphase; with pronounced polar chromosomes comprising ~50% of the total DNA. Notably, these misaligned chromosomes continuously oscillated between the poles and the metaphase plate, as shown in **Fig 4D**.

Consistent with abnormal chromosome dynamics, ~25% of HeLa cells expressing Vif exhibited multi-polar spindles (>2 poles) at 72h post-infection based on fixed cell analysis (**Fig S4C**). To corroborate these findings, we used high-temporal live cell imaging to track and quantify spindle poles using mNeonGreen-Tubulin in Cal51 cells. We observed that ~80% of cells expressing Vif demonstrated multi-polarity at some time point during the extended mitosis. Moreover, the number of spindle poles varied dramatically in arrested cells, ranging from a monopole to as many as five poles (**Fig 4E and S4D**).

The integrity of spindle poles is crucial for maintaining the position of the metaphase plate during mitotic progression, so that the length of microtubules making up the mitotic spindle is tightly regulated and typically remains stable until anaphase onset. Interestingly, we found that mitotic spindles in Vif-expressing cells were significantly stretched (~18 µm in length) as

compared to Control cells (~12 µm) (**Fig 4F and S4E**). Moreover, although mitotic spindles are typically stationary, we observed spindles in Vif-expressing cells to exhibit dynamic spinning. To define these observations quantitatively, we measured the average angle swept by individual mitotic spindles over time in the presence or absence of Vif expression, observing a greater than 15-fold increase in the angle covered by spindles in Vif-expressing cells as compared to Control cells (**Fig 4G and S4F**). In summary, Vif induces dynamic movements in both chromosomes and spindle poles during extended pseudo-metaphase, resulting in severely misaligned polar chromosomes.

Vif, but not Vpr, disrupts proper localization of PP2A-B56 to kinetochores

Microtubule assembly at the kinetochore is regulated by an intricate network of kinase and phosphatases (Saurin, 2018). PP2A-B56 is recruited to kinetochores during prometaphase, where it plays a crucial role in microtubule assembly and the proper alignment of chromosomes (Foley *et al*, 2013; Foley *et al*, 2011a). Previous studies have shown that Vif can degrade B56 proteins (Greenwood *et al.*, 2016; Marelli *et al.*, 2020; Nagata *et al.*, 2020). PP2A-B56 predominantly functions at kinetochores during early mitosis, likely utilizing only a small subset of the total PP2A-B56 since kinetochores are small, nano-scale protein architectures (~250 nm) on mitotic chromosomes. To investigate whether PP2A-B56 levels at kinetochores are reduced

in Vif-expressing cells, we conducted quantitative immunofluorescent (qIF) using specific antibodies against B56 and CENP-C (a kinetochore marker) in Control, Vif-expressing, and Vpr-expressing cells. Our results showed that B56 signals at kinetochores, regardless of whether the chromosomes were aligned (equatorial) or unaligned (polar), were significantly reduced in Vif-expressing cells compared to Control and Vpr-expressing cells (**Fig 5A-C**). To determine if Vif-expressing cells remained free of additional, non-kinetochore-bound pools of B56, we performed qIF in nocodazole-treated cells. Nocodazole, a microtubule depolymerizer, has been shown to enhance B56's localization to the kinetochore (Foley *et al*, 2011b). As expected, Control cells displayed further recruitment of B56 to kinetochores upon nocodazole treatment, whereas Vif-expressing cells did not (**Fig 5A and 5C**).

To further validate these results, we performed qIF using a Polo-like kinase 1 (Plk1) antibody. Plk1 is a key cell cycle regulator, with critical roles at kinetochores in proper mitotic progression (Colicino & Hehnly, 2018). It is known that Plk1 levels at kinetochores are regulated by PP2A-B56, and depletion of B56 leads to increased levels of Plk1 at kinetochores, resulting in improper microtubule attachments (Foley *et al.*, 2011a). As expected, Plk1 levels at kinetochores were significantly decreased in metaphase as compared to prometaphase in Control cells (**Fig 5D-E**). By contrast, Vif-expressing cells exhibited a global increase in Plk1 levels at kinetochores. In summary, Vif, but not Vpr, significantly diminished PP2A-B56 levels at

kinetochores, suggesting that Vif's perturbation of PP2A function likely causes the delay in chromosome alignment, underpinning our observations of Vif-induced pseudo-metaphase arrest.

Vif impairs stable and balanced kinetochore microtubule attachments

We demonstrated that Vif-expressing cells exhibited abnormal dynamic chromosome movements (**Fig 4C-D**). Kinetochore-microtubule bindings are cooperatively stabilized by both PP2-B56 and PP1 at kinetochores through an interplay and feedback mechanism (Saurin, 2018; Vallardi *et al*, 2017). Consequently, we hypothesized that the reduction of PP2A-B56 by Vif impaired the regulation PP1 phosphatase activities at kinetochores. To test this hypothesis, we quantified the levels of the Astrin-SKAP complex (hereinafter referred to as 'Astrin') at kinetochores by qIF in HeLa cells in the presence or absence of Vif expression. Astrin stabilizes kinetochore-microtubule attachments by recruiting PP1, which dephosphorylates Hec1, a microtubule binding protein at kinetochores, thereby promoting Hec1 binding to microtubules (Cheeseman *et al*, 2006; Conti *et al*, 2019; Dunsch *et al*, 2011; Manning *et al*, 2010; Schmidt *et al*, 2010; Zhang *et al*, 2015). As expected, Astrin signals at kinetochores significantly increased at metaphase compared to prometaphase in Control cells (**Fig 6A-B**). In contrast, Astrin levels at kinetochores on aligned chromosomes (equatorial) in Vif-expressing cells were

approximately 50% of control, and Astrin levels on polar chromosomes largely undetectable (**Fig 6A-B**). We confirmed that levels of CENP-C, which is a core-structural kinetochore protein, did not change between Control and Vif-expressing cells, indicating that the reduction of Astrin in Vif-expressing cells was not due to decreased recruitment of core-kinetochore proteins (**Fig 6A-B**).

Generating uniform pulling force across sister kinetochores is essential for maintaining chromosome alignment at the cell equator during metaphase. While control cells showed equal Astrin recruitment at sister kinetochores, consistent with balanced forces (**Fig 6C)**, Vif-expressing cells showed significant differences in Astrin levels between sister kinetochores despite CENP-C levels remaining consistent (**Fig 6C)**.

The N-terminal domain of Hec1 has multiple phosphorylation sites, and dephosphorylation specifically by PP1 is critical for stabilizing its binding to microtubules (DeLuca *et al*, 2011). To directly validate the reduced activity of PP1 at kinetochores in Vif-expressing cells, we performed qIF using a phospho-Hec1 antibody (pS55). As expected, phosphorylation levels of Hec1 (pS55) were high in Control prometaphase and significantly reduced in metaphase (**Fig 6D-E**). In contrast, Hec1 phosphorylation levels remained significantly high at aligned chromosomes (equatorial) in Vif-expressing cells compared to aligned metaphase chromosomes in Control cells (**Fig 6D-E**). Similarly, unaligned

chromosomes (Polar) maintained Hec1 phosphorylation levels similar to those in Control prometaphase. We confirmed that Hec1 levels at kinetochores were the same in both Vif-expressing and Control cells (**Fig 6G-H**). These results demonstrate that PP1 activity at kinetochores is weaker in Vif-expressing cells compared to Control cells. In agreement with the unbalanced Astrin recruitment at sister kinetochores in Vif-expressing cells, Hec1 phosphorylation levels between sister kinetochores were also significantly unbalanced in Vif-expressing cells compared to Control cells (**Fig 6F**). In summary, Vif disrupts the proper assembly of the Astrin-PP1 complex at kinetochores, resulting in the retentions of a high phosphorylation status at Hec1. This leads to weakened and uneven forces between sister kinetochores, likely contributing to dynamic chromosome movements.

Discussion

The specific processes by which HIV-1 causes loss of CD4+ T cells are numerous and include activation of innate immune sensors (Doitsh & Greene, 2016), Envelope-driven cell fusion/syncytiation (Nardacci et al, 2015), and induction of cell cycle arrest followed by programmed cell death mediated by viral gene products that include Vif and Vpr (Muthumani et al, 2005). Vif has recently been shown to induce cell cycle arrest in conjunction with its downregulation of PP2A-B56 subunits (Marelli et al., 2020; Nagata et al., 2020; Salamango et

al., 2019). However, the specific nature of this arrest was not previously examined at the level of single cells and had been assumed to occur during G2 based on flow cytometric assays. In our study, we discovered that expression of Vif actually reduces the duration of G2 (**Fig 3B**) and instead triggers a robust pseudo-metaphase arrest, confirmed in a broad range of cell lines, and with cells typically succumbing to apoptotic cell death after extended pseudo-metaphase (**Fig 1C, 1H, S1E, S2C**). We also demonstrate that, contrary to a prior study (Izumi et al., 2010), Vif-induced pseudo-metaphase arrest occurs independently of p53 status (**Fig 3D-F and S3D-F**).

Further, we demonstrate that Vif specifically disrupts the kinetochore functions, impairing proper mitotic progression. Normally, after NEBD, microtubules efficiently capture kinetochores during prometaphase through the interplay of PP1 and PP2A-B56 phosphatase activities (Sivakumar & Gorbsky, 2017; Smith *et al*, 2019; Vallardi *et al.*, 2017). PP2A-B56 is recruited to kinetochores in prometaphase, reducing Plk1 activity to facilitate kinetochore-microtubule assembly and promoting recruitment of PP1 by multiple adaptors. A major PP1 adaptor for kinetochore recruitment is the Astrin-SKAP complex whose recruitment requires proper microtubule end-on attachment (Conti *et al.*, 2019; Friese *et al*, 2016; McVey *et al*, 2021). In Vif-expressing cells, Vif significantly reduced the level of PP2A-B56 at kinetochore in prometaphase, likely due to its role in B56 degradation. This reduction leads to a slower

establishment of metaphase plate (**Fig 7**). The significant loss of PP2A-B56 at kinetochores impairs the feedback control necessary for stabilizing microtubule binding. As a result, there is a significantly lower and uneven recruitment of Astrin-SKAP-PP1 complex to kinetochores, causing uneven pulling forces between sister chromatids that result in some chromosomes being prematurely pulled towards spindle poles prior to satisfying the mitotic checkpoint (**Fig 7, Step 1**). Upon approaching the spindle poles, Aurora A, another key kinase that regulates mitotic error correction, phosphorylates the MTBDs of Ndc80/Hec1 and destabilizes kinetochore-microtubule attachment (**Fig 7, Step 2**) (Anna *et al*, 2015; Barr & Gergely, 2007; Chmátal *et al*, 2015; DeLuca, 2017; DeLuca *et al.*, 2011; Kettenbach *et al*, 2011). This destabilization of could explain why polar chromosomes in Vif-expressing cells lose Astrin signals at kinetochores (**Fig 6A-B**). Polar chromosomes are then transported back to the equator by polar-ejection forces (**Fig 7, Step 3**) (Poser et al, 2019; Wandke et al, 2012). The repetition of this cycle accounts for the observed abnormal dynamics of chromosome movements in Vif-expressing cells.

Acknowledgement

We would like to thank Yuhi Hara, Takanori Tsuchiya, and Tokai Hit for critical equipment and technical support. We also would like to thank Dr. James Bruce for the critical suggestions and experimental support and Ms. Ainslie Homan for support in data analysis. Part of this work is supported by Wisconsin Partnership Program, the University of Wisconsin-Madison Office of the Vice Chancellor for Research with funding from the Wisconsin Alumni Research Foundation (Research Forward), start-up funding from University of Wisconsin-Madison SMPH, UW Carbone Cancer Center, and McArdle Laboratory for Cancer Research, and NIH grant R35GM147525 (to A.S.) and U54AI170660, R01AI110221, and P01CA022443 (to N.S.).

Author contribution

E.L.E. III initiated the project, identified Vif-induced metaphase arrest, and generated key viral reagents and Vif expression vectors. D.G. conducted the bulk of the follow-up precision imaging

experiments and analyses, with assistance from M.B., K.G.S., N.S., and A.S.. A.S. and N.S. conceptualized, supervised and funded the project. D.G. and A.S. prepared the initial manuscript draft, with assistance from N.S., E.L.E. III, and M.B. All authors reviewed and contributed to the manuscript's refinement.

Competing Financial Interests

The authors declare no further conflict of interests.

Methods

Cell Culture

Human HeLa, RPE1, Cal51, and MDA-MB-231 cells were originally obtained from the American Type Culture Collection (ATCC, Manassas, VA, USA). RPE1 p53 KO, HCT116 p53 KO, RPE1 (H2B-RFP), MDA-MB-231 (H2B-mCherry), and Cal51 (Tubulin-mNeonGreen and H2B-mScarlet were endogenously tagged by CRISPR-Cas9) cells were originally obtained from Dr. Jan Korbel, Dr. Yue Xiong (UNC), Dr. Mark Burkard, and Dr. Beth Weaver, respectively. H2B-GFP expressing HeLa cells and conditional CO-Vif-expressing HeLa cells using a pCEP4 vector (Thermo) containing the TRE and Tet promotor with codon-optimized Vif or mNeonGreen were generated in this study. HeLa, MDA-MB-231, HCT116, RPE1 and Cal51 were grown in

DMEM high glucose (Cytiva Hyclone; SH 30243.01) or DMEM/F12 (Cytiva Hyclone; SH 3026101) supplemented with 1% penicillin-streptomycin, 1% L-glutamine, and 10% fetal bovine serum under 5% CO_2 at 37ºC in an incubator.

Live cell imaging

RPE1, Cal51, HeLa, and MDA-MB-231 cells were plated on 4-chamber 35mm glass bottom dishes at least one day prior to imaging (4 chamber with #1.5 glass, Cellvis). In a subset of experiments, cells were stained using sirDNA (Cytoskeleton, 150 nM) for 2 hours prior to imaging to visualize chromosomal DNA. For conditionally Vif-expressing cells, doxycycline (1 µg/ml, Sigma) was supplemented prior to imaging. High temporal resolution live-cell imaging was performed using a Nikon Ti2 inverted microscope equipped with a Hamamatsu Fusion camera, spectra-X LED light source (Lumencor), Shiraito PureBox (TokaiHit), and a Plan Apo 20x objective (NA = 0.75) controlled by Nikon Elements software. Cells were recorded at 37°C with 5% CO2 in a stage-top incubator using the feedback control function to accurately maintain temperature of growth medium (Tokai Hit, STX model). Images were recorded for 48-120 hours at 6-12 min intervals with three to four z-stack images acquired at steps of 1.5~2 µm for each time point.

Fixed high- and super-resolution imaging

HeLa cells infected “Control” (Vif-negative) and Vif-containing viruses were fixed by 4% PFA (Sigma) at 72 hours post-infection. Cells were then permeabilized by 0.5% NP40 (Sigma) and incubated with 0.5% BSA (Sigma). Following primary and secondary antibodies were used; CENP-C (MBL), Tubulin (Sigma), GFP (Thermo), B56-alpha (BD Biosciences), Plk1 (Santa Cruz), Astrin (Sigma), Hec1/9G3 (Abcam), Hec1 pS55 (GeneTex), anti-mouse IgG Alexa 488 (min X, JacksonImmuno research), anti-guinea pig IgG Rhodamine Red X (min X, Jackson immune research), anti-guinea pig IgG Alexa 647 (min X, JacksonImmuno research), anti-rabbit IgG Alexa-488 (JacksonImmuno research) and anti-rabbit Alexa 647 (min X, Jackson immune research). Stained samples were imaged both CSU W1 spinning disc confocal and CSU W1 SoRa super-resolution (Yokogawa) confocal microscope (Loi et al, 2023). These spinning disc confocal units were equipped with a Nikon Ti2 inverted microscope with a Hamamatsu Fusion camera, Shiraito PureBox (TokaiHit), and a TIRF SR 100x objective (NA = 1.49). The microscope system was controlled by Nikon Elements software (Nikon). Figure 3B images were generated using Imaris software (Andor).

Image analysis

Image analysis was performed using Nikon Elements software (Nikon) or Metamorph

(Molecular Devices). Mitotic stages and errors were determined by nuclear staining. The mitotic duration was defined as the time from nuclear envelope breakdown (NEBD) to anaphase onset. Incidences of multi-nuclei, mitotic slippages, lagging chromosomes, unaligned chromosome, and chromosome bridges were documented. CFP signals were used as a marker for infected cells. Tubulin-mNeonGreen was used for quantifying numbers of spindle poles and monitoring their dynamics. Spindle pole distance was measured when spindle poles were maximally stretched in high-temporal live cell images using Nikon Elements.

Cell cycle phase analysis

To track cell cycle progression, H2B signals were measured over time using Nikon NIS Elements on time lapse images of Cal51 cells. Signal intensities were measured manually and the local background correction method (Loi *et al.*, 2023; Suzuki *et al*, 2015) was applied to accurately quantify chromatin signal intensity. Signals were collected in this manner at 18-30 min intervals. Each cell cycle stage was defined based on the nature and intensity of the H2B-mScarlet signal.

Polar chromosome quantification

Cell segmentation and measurements of chromosome distribution were performed using the

Nikon NIS Elements program. First, the region-of-interest (ROI) tool was used to select chromosomes located at each pole or at the equator. Corrected signal intensity was calculated using a local background correction method. Measurements were made for every 6 minutes for the first 2 hours after NEBD, and for every ~1.5 hours subsequently. For each time point, the percentage of polar chromosomes was calculated using the following formula: (Corrected intensity of Pole1+Pole2)*100/(Corrected intensity of Pole1+Pole2+Equator).

Spindle rotation measurements

Measurements of spindle rotation were performed using the Nikon Elements program's Manual Measurement tool. Cells were observed after NEBD and the free angle tool was used to measure the absolute value of the spindle rotation angle traced from either the longitudinal axis or using equatorial chromosomes as a reference. For control cells, measurements were made for each consecutive frame from the first frame where a spindle appeared until the first frame at the onset of anaphase. By contrast, for Vif-expressing cells measurements were made for frames whenever a visually significant angle was traced. Data was exported to Excel. The Matplotlib library in Python was used to make polar plots, with time plotted as radius and angle traced plotted as theta.

Statistics

All experiments were independently repeated 2-3 times for mitotic duration measurements. p-values were calculated using one-way ANOVA and the two-tailed Student's t-test. p-values < 0.05 were considered significant.

Transduction and infection

For infections, growth media was replaced with viral supernatants carrying VSV-G-pseudo typed HIV-1 CFP reporter viruses (Vif-positive or Vif-negative) at a multiplicity of infection of ~1, with the viruses engineered and produced as previously described (Evans et al., 2018).

References

Anna AY, Deretic J, Hoel CM, Hinman AW, Cimini D, Welburn JP, Maresca TJ (2015) Aurora A kinase contributes to a pole-based error correction pathway. *Current Biology* 25: 1842-1851

Augustine T, Chaudhary P, Gupta K, Islam S, Ghosh P, Santra MK, Mitra D (2017) Cyclin F/FBXO1 Interacts with HIV-1 Viral Infectivity Factor (Vif) and Restricts Progeny Virion Infectivity by Ubiquitination and Proteasomal Degradation of Vif Protein through SCFcyclin F E3 Ligase Machinery. *Journal of Biological Chemistry* 292: 5349-5363

Barr AR, Gergely F (2007) Aurora-A: the maker and breaker of spindle poles. *Journal of Cell Science* 120: 2987-2996

Bartz SR, Rogel ME, Emerman M (1996) Human immunodeficiency virus type 1 cell cycle control: Vpr is cytostatic and mediates G2 accumulation by a mechanism which differs from DNA damage checkpoint control. *J Virol* 70: 2324-2331

Behrens RT, Sherer NM (2023) Retroviral hijacking of host transport pathways for genome nuclear export. *mBio* 14: e0007023

Cheeseman IM, Chappie JS, Wilson-Kubalek EM, Desai A (2006) The conserved KMN network constitutes the core microtubule-binding site of the kinetochore. *Cell* 127: 983-997

Chiu Y-L, Greene WC (2009) APOBEC3G: an intracellular centurion. *Philosophical Transactions of the Royal Society B: Biological Sciences* 364: 689-703

Chmátal L, Yang K, Schultz RM, Lampson MA (2015) Spatial regulation of kinetochore microtubule attachments by destabilization at spindle poles in meiosis I. *Current Biology* 25: 1835-1841

Choi HJ, Fukui M, Zhu BT (2011) Role of Cyclin B1/Cdc2 Up-Regulation in the Development of Mitotic Prometaphase Arrest in Human Breast Cancer Cells Treated with Nocodazole. *Plos One* 6

Clijsters L, Hoencamp C, Calis JJA, Marzio A, Handgraaf SM, Cuitino MC, Rosenberg BR, Leone G, Pagano M (2019) Cyclin F Controls Cell-Cycle Transcriptional Outputs by Directing the Degradation of the Three Activator E2Fs. *Molecular Cell* 74:

550 1264-1277.e1267
551 Cohen MS, Chen YQ, McCauley M, Gamble T, Hosseinipour MC, Kumarasamy N, Hakim JG, Kumwenda J, Grinsztejn B, Pilotto
552 JHS *et al* (2016) Antiretroviral Therapy for the Prevention of HIV-1 Transmission. *New England Journal of Medicine* 375:
553 830-839
554 Colicino EG, Hehnly H (2018) Regulating a key mitotic regulator, polo-like kinase 1 (PLK1). *Cytoskeleton (Hoboken)* 75:
555 481-494
556 Conti D, Gul P, Islam A, Martín-Durán JM, Pickersgill RW, Draviam VM (2019) Kinetochores attached to microtubule-ends are
557 stabilised by Astrin bound PP1 to ensure proper chromosome segregation. *eLife* 8: e49325
558 Conticello SG, Harris RS, Neuberger MS (2003) The Vif protein of HIV triggers degradation of the human antiretroviral DNA
559 deaminase APOBEC3G. *Current Biology* 13: 2009-2013
560 Das AT, Tenenbaum L, Berkhout B (2016) Tet-On Systems For Doxycycline-inducible Gene Expression. *Curr Gene Ther* 16:
561 156-167
562 Deeks SG, Overbaugh J, Phillips A, Buchbinder S (2015) HIV infection. *Nature Reviews Disease Primers* 1
563 DeHart JL, Bosque A, Harris RS, Planelles V (2008) Human immunodeficiency virus type 1 Vif induces cell cycle delay via
564 recruitment of the same E3 ubiquitin ligase complex that targets APOBEC3 proteins for degradation. *Journal of virology* 82:
565 9265-9272
566 DeLuca JG, 2017. Aurora A kinase function at kinetochores, Cold Spring Harbor Symposia on Quantitative Biology. Cold
567 Spring Harbor Laboratory Press, pp. 91-99.
568 DeLuca KF, Lens SMA, DeLuca JG (2011) Temporal changes in Hec1 phosphorylation control kinetochore–microtubule
569 attachment stability during mitosis. *Journal of Cell Science* 124: 622-634
570 Doitsh G, Greene WC (2016) Dissecting How CD4 T Cells Are Lost During HIV Infection. *Cell Host & Microbe* 19: 280-291
571 Du J, Rui Y, Zheng W, Li P, Kang J, Zhao K, Sun T, Yu X-F (2019) Vif-CBFβ interaction is essential for Vif-induced cell cycle arrest.
572 *Biochemical and biophysical research communications* 511: 910-915
573 Dunsch AK, Linnane E, Barr FA, Gruneberg U (2011) The astrin–kinastrin/SKAP complex localizes to microtubule plus ends
574 and facilitates chromosome alignment. *Journal of Cell Biology* 192: 959-968
575 Elder RT (2002) HIV-1 VPR modulates cell cycle G2/M transition through an alternative cellular mechanism other than the
576 classic mitotic checkpoints. *Frontiers in Bioscience* 7
577 Emerman M (1996) HIV-1, Vpr and the cell cycle. *Current Biology* 6: 1096-1103
578 Enrico TP, Stallaert W, Wick ET, Ngoi P, Wang X, Rubin SM, Brown NG, Purvis JE, Emanuele MJ (2021) Cyclin F drives
579 proliferation through SCF-dependent degradation of the retinoblastoma-like tumor suppressor p130/RBL2. *eLife* 10
580 Evans EL, Becker JT, Fricke SL, Patel K, Sherer NM, Kirchhoff F (2018) HIV-1 Vif's Capacity To Manipulate the Cell Cycle Is
581 Species Specific. *Journal of Virology* 92
582 Foley EA, Magidson V, Khodjakov A, Kapoor T (2013) The B56-PP2A phosphatase is required for the formation of stable
583 attachments between kinetochores and microtubule plus-ends. *Mol Biol Cell* 24
584 Foley EA, Maldonado M, Kapoor TM (2011a) Formation of stable attachments between kinetochores and microtubules
585 depends on the B56-PP2A phosphatase. *Nat Cell Biol* 13: 1265-U1216

586 Foley EA, Maldonado M, Kapoor TM (2011b) Formation of stable attachments between kinetochores and microtubules
587 depends on the B56-PP2A phosphatase. *Nature cell biology* 13: 1265-1271
588 Friese A, Faesen AC, Huis in 't Veld PJ, Fischböck J, Prumbaum D, Petrovic A, Raunser S, Herzog F, Musacchio A (2016)
589 Molecular requirements for the inter-subunit interaction and kinetochore recruitment of SKAP and Astrin. *Nature*
590 *Communications* 7: 11407
591 Gabuzda DH, Lawrence K, Langhoff E, Terwilliger E, Dorfman T, Haseltine WA, Sodroski J (1992) Role of Vif in Replication of
592 Human-Immunodeficiency-Virus Type-1 in Cd4+ T Lymphocytes. *Journal of Virology* 66: 6489-6495
593 Greenwood EJD, Matheson NJ, Wals K, van den Boomen DJH, Antrobus R, Williamson JC, Lehner PJ (2016) Temporal
594 proteomic analysis of HIV infection reveals remodelling of the host phosphoproteome by lentiviral Vif variants. *Elife* 5:
595 e18296
596 Grulich AE, van Leeuwen MT, Falster MO, Vajdic CM (2007) Incidence of cancers in people with HIV/AIDS compared with
597 immunosuppressed transplant recipients: a meta-analysis. *The Lancet* 370: 59-67
598 Hall R, Ahern LM, Yap MW, Tsai M-HC, Boucherit VC, Takaki T, Boulton SJ, Bishop KN (2024) HIV-1 Vpr causes separate cell
599 cycle arrests in G2 and M that activate alternative DNA damage pathways. *bioRxiv*: 2024.2004. 2002.587683
600 He J, Choe S, Walker R, Di Marzio P, Morgan DO, Landau NR (1995) Human immunodeficiency virus type 1 viral protein R
601 (Vpr) arrests cells in the G2 phase of the cell cycle by inhibiting p34cdc2 activity. *J Virol* 69: 6705-6711
602 Hernández-Ramírez RU, Shiels MS, Dubrow R, Engels EA (2017) Cancer risk in HIV-infected people in the USA from 1996 to
603 2012: a population-based, registry-linkage study. *The Lancet HIV* 4: e495-e504
604 Izumi T, Io K, Matsui M, Shirakawa K, Shinohara M, Nagai Y, Kawahara M, Kobayashi M, Kondoh H, Misawa N *et al* (2010)
605 HIV-1 viral infectivity factor interacts with TP53 to induce G2 cell cycle arrest and positively regulate viral replication.
606 *Proceedings of the National Academy of Sciences* 107: 20798-20803
607 Jouvenet N, Simon SM, Bieniasz PD (2009) Imaging the interaction of HIV-1 genomes and Gag during assembly of individual
608 viral particles. *Proceedings of the National Academy of Sciences* 106: 19114-19119
609 Jowett JB, Planelles V, Poon B, Shah NP, Chen ML, Chen IS (1995) The human immunodeficiency virus type 1 vpr gene arrests
610 infected T cells in the G2 + M phase of the cell cycle. *J Virol* 69: 6304-6313
611 Kettenbach AN, Schweppe DK, Faherty BK, Pechenick D, Pletnev AA, Gerber SA (2011) Quantitative Phosphoproteomics
612 Identifies Substrates and Functional Modules of Aurora and Polo-Like Kinase Activities in Mitotic Cells. *Science Signaling* 4:
613 rs5-rs5
614 Lee SJ, Rodriguez-Bravo V, Kim H, Datta S, Foley EA (2017) The PP2AB56 phosphatase promotes the association of Cdc20
615 with APC/C in mitosis. *Journal of cell science*
616 Loi J, Qu X, Suzuki A (2023) Semi-automated 3D fluorescence speckle analyzer (3D-Speckler) for microscope calibration and
617 nanoscale measurement. *The Journal of cell biology* 222
618 Lynch AR, Arp NL, Zhou AS, Weaver BA, Burkard ME (2022) Quantifying chromosomal instability from intratumoral
619 karyotype diversity using agent-based modeling and Bayesian inference. *Elife* 11: e69799
620 Malim MH, Emerman M (2008) HIV-1 accessory proteins—ensuring viral survival in a hostile environment. *Cell host &*
621 *microbe* 3: 388-398

622 Manning AL, Bakhoum SF, Maffini S, Correia - Melo C, Maiato H, Compton DA (2010) CLASP1, astrin and Kif2b form a
623 molecular switch that regulates kinetochore - microtubule dynamics to promote mitotic progression and fidelity. *The EMBO*
624 *Journal* 29: 3531-3543-3543
625 Mardin BR, Drainas AP, Waszak SM, Weischenfeldt J, Isokane M, Stütz AM, Raeder B, Efthymiopoulos T, Buccitelli C,
626 Segura-Wang M *et al* (2015) A cell-based model system links chromothripsis with hyperploidy. *Mol Syst Biol* 11
627 Marelli S, Williamson JC, Protasio AV, Naamati A, Greenwood EJD, Deane JE, Lehner PJ, Matheson NJ (2020) Antagonism of
628 PP2A is an independent and conserved function of HIV-1 Vif and causes cell cycle arrest. *eLife* 9
629 Marin M, Rose KM, Kozak SL, Kabat D (2003) HIV-1 Vif protein binds the editing enzyme APOBEC3G and induces its
630 degradation. *Nature Medicine* 9: 1398-1403
631 McVey SL, Cosby JK, Nannas NJ (2021) Aurora B Tension Sensing Mechanisms in the Kinetochore Ensure Accurate
632 Chromosome Segregation. *Int J Mol Sci* 22
633 Muthumani K, Choo AY, Premkumar A, Hwang DS, Thieu KP, Desai BM, Weiner DB (2005) Human immunodeficiency virus
634 type 1 (HIV-1) Vpr-regulated cell death: insights into mechanism. *Cell Death Differ* 12: 962-970
635 Nagata K, Shindo K, Matsui Y, Shirakawa K, Takaori-Kondo A (2020) Critical role of PP2A-B56 family protein degradation in
636 HIV-1 Vif mediated G2 cell cycle arrest. *Biochemical and biophysical research communications* 527: 257-263
637 Nardacci R, Perfettini JL, Grieco L, Thieffry D, Kroemer G, Piacentini M (2015) Syncytial apoptosis signaling network induced
638 by the HIV-1 envelope glycoprotein complex: an overview. *Cell Death Dis* 6
639 Nguyen DH, Hildreth JEK (2000) Evidence for Budding of Human Immunodeficiency Virus Type 1 Selectively from
640 Glycolipid-Enriched Membrane Lipid Rafts. *Journal of Virology* 74: 3264-3272
641 Okada A, Iwatani Y (2016) APOBEC3G-Mediated G-to-A Hypermutation of the HIV-1 Genome: The Missing Link in Antiviral
642 Molecular Mechanisms. *Frontiers in Microbiology* 7
643 Olivier M, Eeles R, Hollstein M, Khan MA, Harris CC, Hainaut P (2002) The IARC TP53 database: New online mutation analysis
644 and recommendations to users. *Human Mutation* 19: 607-614
645 Ono A, Freed EO (2001) Plasma membrane rafts play a critical role in HIV-1 assembly and release. *Proceedings of the*
646 *National Academy of Sciences* 98: 13925-13930
647 Parkin DM (2006) The global health burden of infection-associated cancers in the year 2002. *Int J Cancer* 118: 3030-3044
648 Poser E, Caous R, Gruneberg U, Barr FA (2019) Aurora A promotes chromosome congression by activating the
649 condensin-dependent pool of KIF4A. *Journal of Cell Biology* 219
650 Sakai K, Barnitz RA, Chaigne-Delalande B, Bidère N, Lenardo MJ (2011) Human Immunodeficiency Virus Type 1 Vif causes
651 dysfunction of Cdk1 and CyclinB1: implications for cell cycle arrest. *Virology Journal* 8
652 Sakai K, Dimas J, Lenardo MJ (2006) The Vif and Vpr accessory proteins independently cause HIV-1-induced T cell
653 cytopathicity and cell cycle arrest. *Proceedings of the National Academy of Sciences* 103: 3369-3374
654 Salamango DJ, Ikeda T, Moghadasi SA, Wang J, McCann JL, Serebrenik AA, Ebrahimi D, Jarvis MC, Brown WL, Harris RS (2019)
655 HIV-1 Vif Triggers Cell Cycle Arrest by Degrading Cellular PPP2R5 Phospho-regulators. *Cell Reports* 29: 1057-1065.e1054
656 Salamango DJ, McCann JL, Demir Ö, Becker JT, Wang J, Lingappa JR, Temiz NA, Brown WL, Amaro RE, Harris RS *et al* (2020)
657 Functional and Structural Insights into a Vif/PPP2R5 Complex Elucidated Using Patient HIV-1 Isolates and Computational

658 Modeling. *Journal of Virology* 94
659 Saurin AT (2018) Kinase and Phosphatase Cross-Talk at the Kinetochore. *Front Cell Dev Biol* 6: 62
660 Schmidt JC, Kiyomitsu T, Hori T, Backer CB, Fukagawa T, Cheeseman IM (2010) Aurora B kinase controls the targeting of the
661 Astrin–SKAP complex to bioriented kinetochores. *Journal of Cell Biology* 191: 269-280
662 Schuhmacher D, Sontag J-M, Sontag E (2019) Protein Phosphatase 2A: More Than a Passenger in the Regulation of Epithelial
663 Cell–Cell Junctions. *Frontiers in Cell and Developmental Biology* 7
664 Scribano CM, Wan J, Esbona K, Tucker JB, Lasek A, Zhou AS, Zasadil LM, Molini R, Fitzgerald J, Lager AM *et al* (2021)
665 Chromosomal instability sensitizes patient breast tumors to multipolar divisions induced by paclitaxel. *Science Translational*
666 *Medicine* 13
667 Sheehy AM, Gaddis NC, Malim MH (2003) The antiretroviral enzyme APOBEC3G is degraded by the proteasome in response
668 to HIV-1 Vif. *Nature Medicine* 9: 1404-1407
669 Sivakumar S, Gorbsky GJ (2017) Phosphatase-regulated recruitment of the spindle- and kinetochore-associated (Ska)
670 complex to kinetochores. *Biol Open* 6: 1672-1679
671 Smith RJ, Cordeiro MH, Davey NE, Vallardi G, Ciliberto A, Gross F, Saurin AT (2019) PP1 and PP2A Use Opposite
672 Phospho-dependencies to Control Distinct Processes at the Kinetochore. *Cell Rep* 28: 2206-2219 e2208
673 St Clair S, Giono L, Varmeh-Ziaie S, Resnick-Silverman L, Liu WJ, Padi A, Dastidar J, DaCosta A, Mattia M, Manfredi JJ (2004)
674 DNA damage-induced downregulation of Cdc25C is mediated by p53 via two independent mechanisms:: One involves direct
675 binding to the
676 promoter. *Molecular Cell* 16: 725-736
677 Stark GR, Taylor WR (2006) Control of the G2/M transition. *Molecular Biotechnology* 32: 227-248
678 Stopak K, de Noronha C, Yonemoto W, Greene WC (2003) HIV-1 Vif blocks the antiviral activity of APOBEC3G by impairing
679 both its translation and intracellular stability. *Molecular cell* 12: 591-601
680 Suzuki A, Badger BL, Salmon ED (2015) A quantitative description of Ndc80 complex linkage to human kinetochores. *Nature*
681 *communications* 6: 8161
682 Swanstrom R, Coffin J (2012) HIV-1 Pathogenesis: The Virus. *Cold Spring Harbor Perspectives in Medicine* 2:
683 a007443-a007443
684 Taylor WR, Stark GR (2001) Regulation of the G2/M transition by p53. *Oncogene* 20: 1803-1815
685 Vallardi G, Cordeiro MH, Saurin AT (2017) A Kinase-Phosphatase Network that Regulates Kinetochore-Microtubule
686 Attachments and the SAC. *Prog Mol Subcell Biol* 56: 457-484
687 Wandke C, Barisic M, Sigl R, Rauch V, Wolf F, Amaro AC, Tan CH, Pereira AJ, Kutay U, Maiato H *et al* (2012) Human
688 chromokinesins promote chromosome congression and spindle microtubule dynamics during mitosis. *Journal of Cell Biology*
689 198: 847-863
690 Wang J, Reuschel EL, Shackelford JM, Jeang L, Shivers DK, Diehl JA, Yu X-F, Finkel TH (2011) HIV-1 Vif promotes the G1- to
691 S-phase cell-cycle transition. *Blood* 117: 1260-1269
692 Wang J, Shackelford JM, Selliah N, Shivers DK, O'Neill E, Garcia JV, Muthumani K, Weiner D, Yu X-F, Gabuzda D *et al* (2008)
693 The HIV-1 Vif Protein Mediates Degradation of Vpr and Reduces Vpr-Induced Cell Cycle Arrest. *DNA and Cell Biology* 27:

694 267-277
695 Yu X, Yu Y, Liu B, Luo K, Kong W, Mao P, Yu X-F (2003) Induction of APOBEC3G Ubiquitination and Degradation by an HIV-1
696 Vif-Cul5-SCF Complex. *Science* 302: 1056-1060
697 Zhang P, Zhang Y, Gao K, Wang Y, Jin X, Wei Y, Saiyin H, Wang D, Peng J, Ma J *et al* (2015) ASPP1/2-PP1 complexes are
698 required for chromosome segregation and kinetochore-microtubule attachments. *Oncotarget* 6: 41550-41565
699 Zhao K, Du J, Rui Y, Zheng W, Kang J, Hou J, Wang K, Zhang W, Simon VA, Yu X-F (2015) Evolutionarily conserved pressure for
700 the existence of distinct G2/M cell cycle arrest and A3H inactivation functions in HIV-1 Vif. *Cell cycle* 14: 838-847

701

702

Figure Legends

Figure 1: Vif and Vpr induce distinct forms of mitotic arrest.

(A) Representative live cell image for Cal51 cells with H2B-mScarlet and Tubulin-mNeonGreen expressing Control, Vif, Vpr, or Vif+Vpr reporter viruses. (B) Average mitotic duration of Cal51 cells expressing respective reporter virus (n=100 for each from two replicates). (C) Frequency of cell fate after mitosis for Cal51 cells expressing respective reporter virus. (n=100 for each from two replicates)

Figure 2: Vif induces robust pseudo-metaphase arrest.

(A) Representative live cell images for Cal51 cells with H2B-mScarlet and Tubulin-mNeonGreen expressing Control reporter virus. (B) Representative live cell image for Cal51 cells expressing Vif reporter virus. (C) Frequency of cells that achieve metaphase plate and time taken to achieve metaphase plate for cells in (A) and (B) (n=100 for each from two replicates). (D) Representative live-cell images of Vif conditional expressed HeLa cell with or without Doxycycline (Dox). (E) Average mitotic duration in condition (D) (n=100 cells for each from two replicates). (F) Quantification of viable cells over time after Dox induction. (G) Quantification of apoptotic cells after Dox induction.

Figure 3: Vif does not alter G1 or S phase progression, accelerates G2 progression, and induces pseudo-metaphase arrest independent of p53

(A) Top: Representative image of Cal51 cells progressing through G1, S, and G2. Bottom: Representative trace for relative signal intensity of the nucleus through cell cycle. (B) Average duration of G1, S, and G2 phases in Control and Vif-expressing cells (n= 9 for Control and 11 for Vif, from two replicates). (C) Total cell cycle duration for Control and Vif-expressing cells. (D) Representative live cell images for Control and Vif-expressing WT or p35KO RPE1 cells. (E) Average mitotic duration in WT or p53KO RPE1 cells (n= >85 cells, from two replicates). (F) Frequency of cells which achieve metaphase plate for cells in (E). (G) Average time taken to achieve metaphase plate for cells in (F).

Figure 4: Vif induces polar chromosomes, multi-polar spindles, and abnormal chromosome movements

(A) Representative immunofluorescence images labeled for CENP-C (as a kinetochore marker), microtubule, and DNA in Control and Vif-expressing HeLa cells. (B) Example super-resolution images labeled for CENP-C, microtubule, and DNA in Vif-expressed HeLa cells showing polar chromosomes. (C) Representative live cell image of Vif-expressing cells where polar chromosomes were quantified by compartmentalizing polar regions. Bottom:

Quantification of polar chromosome frequency overtime. (D) Representative high-temporal live cell images (6 minutes interval) showing rapid chromosome moving towards and away from the spindle poles. (E) Fraction of Cal51 cells showing abnormal number of poles at some point during mitosis. (F) Top: Representative images of maximum mitotic spindle length for Control and Vif-expressing Cal51 cells. Bottom: Average maximum mitotic spindle length of Control and Vif-expressing cells. (G) Top: Representative live cell image of Control and Vif-expressing Cal51 cells over time showing dynamic spindle spinning. Center: Representative figures showing relative orientation (angle) of the spindle axis over time (radius). Bottom: Average total angle swept during mitosis.

Figure 5: Vif, but not Vpr, disrupts the proper localization of PP2A-B56 at the kinetochores

(A) Representative immunofluorescence images labeled B56, CENP-C, and DNA in Control and Vif-expressing HeLa cells with or without nocodazole treatment. (B) Representative immunofluorescence images labeled B56, CENP-C, and DNA in Control and Vpr-expressing HeLa cells. (C) Normalized B56 intensities at kinetochores for cells in (A) and (B) (n=200 kinetochores over 8 cells from two independent replicates for each). (D) Representative immunofluorescence images labeled for Plk1, CENP-C, and DNA of Control HeLa cells and

cells expressing Vif. (E) Normalized Plk1 intensities at kinetochore for cells in (D) (n=200 kinetochores over 8 cells from two independent replicates for each).

Figure 6: Vif impairs stable and balanced kinetochore microtubule attachments

(A) Left: Representative immunofluorescence images labeled CENP-C, Astrin, and DNA in Control and Vif-expressing HeLa cells, Right: Illustrative interpretation of images on the left. (B) Normalized Astrin and CENP-C intensities at kinetochores for cells in (A) (n = 200 kinetochores from 8 cells from two independent replicates for each) (C) Relative signal intensities of Astrin and CENP-C between sister kinetochores, values normalized with formula: 1 – (lower intensity value/higher intensity value). (D) Representative immunofluorescence images labeled for CENP-C, pHec1(S55), and DNA in Control and Vif-expressing HeLa cells. (E) Normalized pHec1(S55) intensities at kinetochores for cells in (D). (n = 200 kinetochores from 8 cells from two independent replicates for each). (F) Relative pHec1(S55) intensities between sister kinetochores, values normalized with formula: 1 – (lower intensity value/higher intensity value). (G) Representative immunofluorescence images labeled for Hec1, CENP-C, and DNA in HeLa cells expressing Vif. (H) Normalized Hec1 intensities at kinetochores for cells in (G) (n=200 kinetochores over 8 cells from two independent replicates for each).

Figure 7: Proposed model for the molecular mechanism underlying Vif's pseudo-metaphase arrest

Top: Cartoon model depicting metaphase alignment of Control cells followed by anaphase. Middle: Cartoon model depicting pseudo-metaphase alignment of Vif-expressing cells with unbalanced microtubule attachment followed by three-step polar chromosome cycle. Bottom: Cartoon depiction of three-step polar chromosome cycle, (1) chromosome at the equator is pulled towards pole due to unbalanced pulling force, (2) kinetochore-microtubule destabilization at the spindle pole, (3) equator-directed movement of chromosome for realignment.

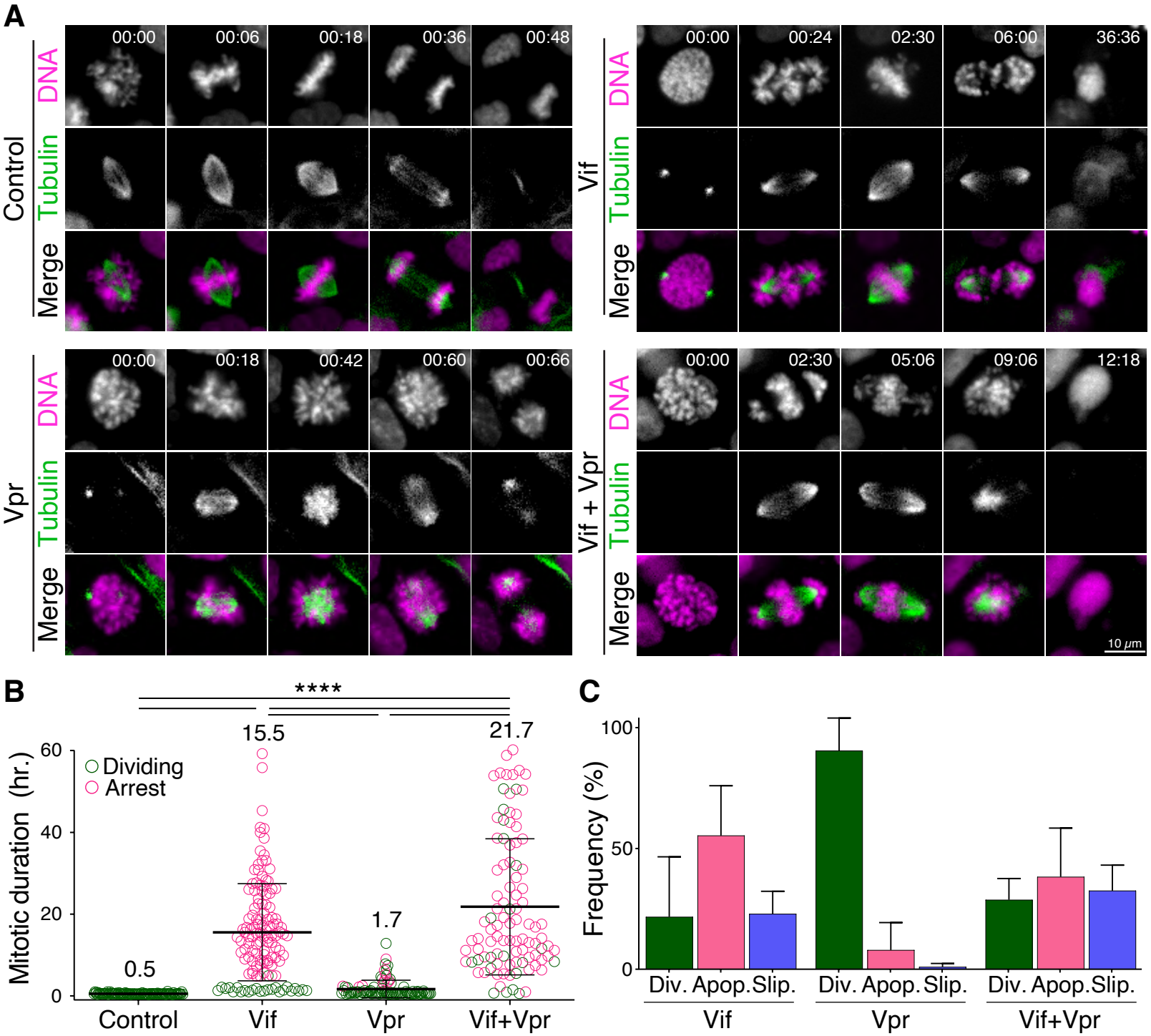
A
Control
Vif
Vpr
Vif + Vpr
DNA
Tubulin
Merge
00:00
00:06
00:18
00:36
00:48
00:24
02:30
06:00
36:36
00:42
00:60
00:66
05:06
09:06
12:18
10 μm
B
****
Mitotic duration (hr.)
Dividing
Arrest
0.5
15.5
1.7
21.7
Control
Vif
Vpr
Vif+Vpr
C
Frequency (%)
Div.
Apop.
Slip.

Figure 1

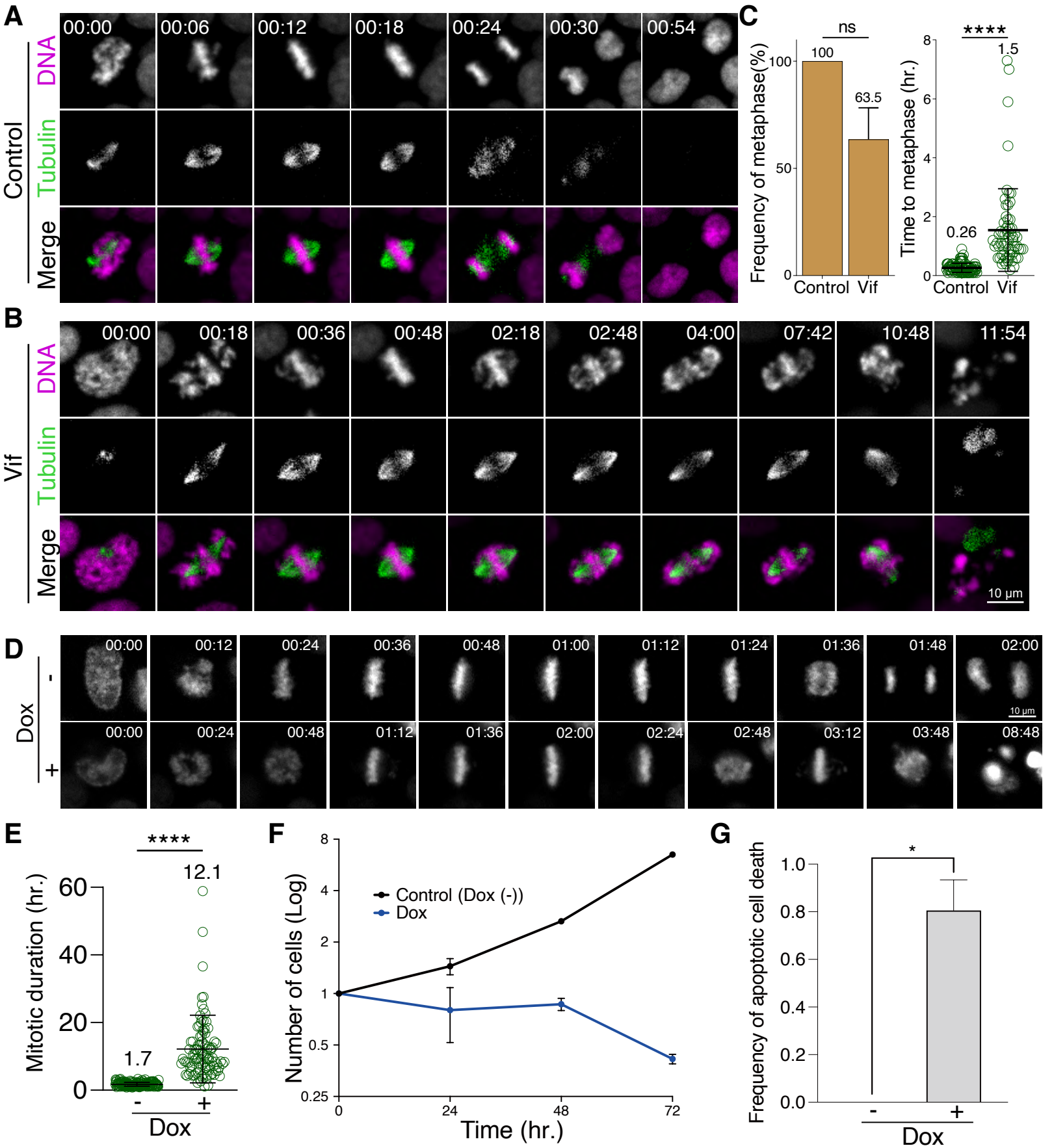
A
Control
DNA
Tubulin
Merge
00:00
00:06
00:12
00:18
00:24
00:30
00:54
B
Vif
00:00
00:18
00:36
00:48
02:18
02:48
04:00
07:42
10:48
11:54
10 µm
C
ns
100
63.5
Frequency of metaphase(%)
Control
Vif
****
1.5
0.26
Time to metaphase (hr.)
D
Dox
-
+
00:00
00:12
00:24
00:36
00:48
01:00
01:12
01:24
01:36
01:48
02:00
10 µm
00:00
00:24
00:48
01:12
01:36
02:00
02:24
02:48
03:12
03:48
08:48
E
****
12.1
1.7
Mitotic duration (hr.)
Dox
F
Control (Dox (-))
Dox
Number of cells (Log)
Time (hr.)
G
*
Frequency of apoptotic cell death
Dox

Figure 2

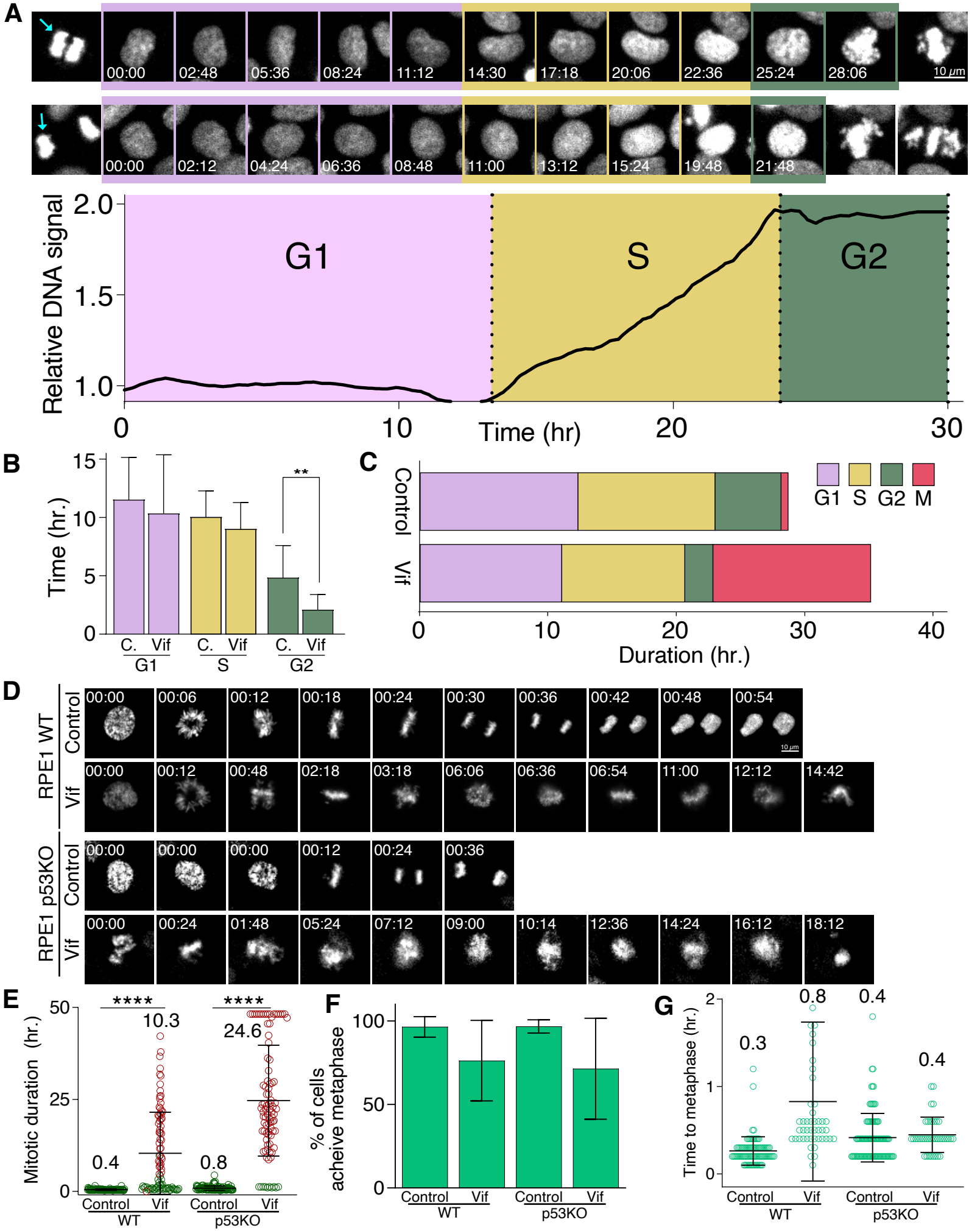
A
00:00
02:48
05:36
08:24
11:12
14:30
17:18
20:06
22:36
25:24
28:06
10 μm
00:00
02:12
04:24
06:36
08:48
11:00
13:12
15:24
19:48
21:48
Relative DNA signal
2.0
1.5
1.0
G1
S
G2
0
10
20
30
Time (hr)
B
Time (hr.)
15
10
5
0
**
C. Vif
G1
S
G2
C
Control
Vif
G1 S G2 M
0
10
20
30
40
Duration (hr.)
D
RPE1 WT
Control
00:00
00:06
00:12
00:18
00:24
00:30
00:36
00:42
00:48
00:54
10 μm
Vif
00:00
00:12
00:48
02:18
03:18
06:06
06:36
06:54
11:00
12:12
14:42
RPE1 p53KO
Control
00:00
00:00
00:00
00:12
00:24
00:36
Vif
00:00
00:24
01:48
05:24
07:12
09:00
10:14
12:36
14:24
16:12
18:12
E
Mitotic duration (hr.)
50
25
0
****
10.3
0.4
****
24.6
0.8
Control
Vif
WT
p53KO
F
% of cells acheive metaphase
100
50
0
Control
Vif
WT
p53KO
G
Time to metaphase (hr.)
2
1
0
0.3
0.8
0.4
0.4
Control
Vif
WT
p53KO

Figure 3

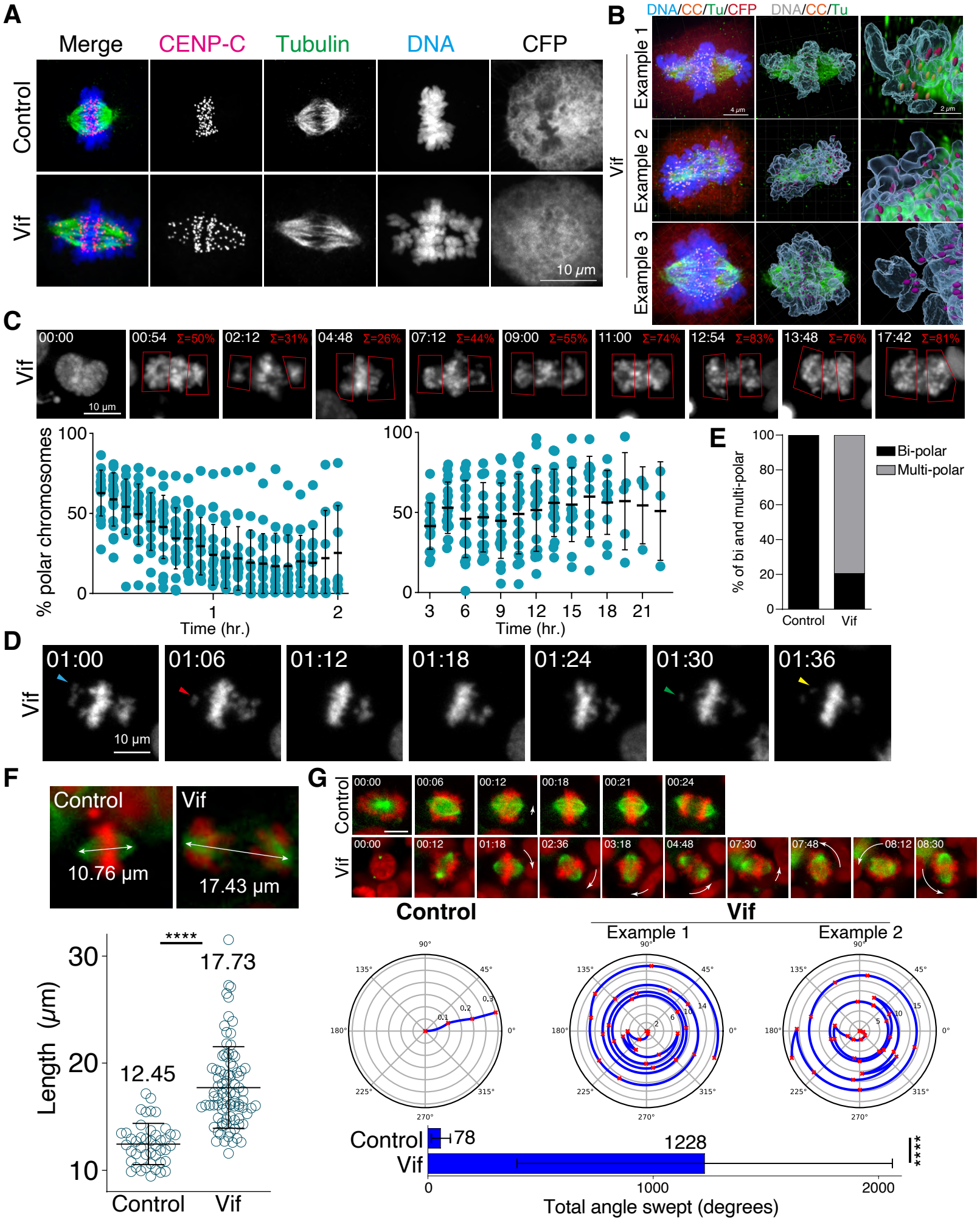
A
Merge
CENP-C
Tubulin
DNA
CFP
Control
Vif
10 μm
B
DNA/CC/Tu/CFP
DNA/CC/Tu
Example 1
Example 2
Example 3
Vif
4 μm
2 μm
C
Vif
00:00
00:54 Σ=50%
02:12 Σ=31%
04:48 Σ=26%
07:12 Σ=44%
09:00 Σ=55%
11:00 Σ=74%
12:54 Σ=83%
13:48 Σ=76%
17:42 Σ=81%
10 μm
% polar chromosomes
Time (hr.)
E
% of bi and multi-polar
Bi-polar
Multi-polar
Control
Vif
D
Vif
01:00
01:06
01:12
01:18
01:24
01:30
01:36
10 μm
F
Control
Vif
10.76 μm
17.43 μm
Length (μm)
****
12.45
17.73
Control
Vif
G
Control
Vif
00:00
00:06
00:12
00:18
00:21
00:24
00:12
01:18
02:36
03:18
04:48
07:30
07:48
08:12
08:30
Control
Vif
Example 1
Example 2
Control
Vif
78
1228
****
Total angle swept (degrees)

Figure 4

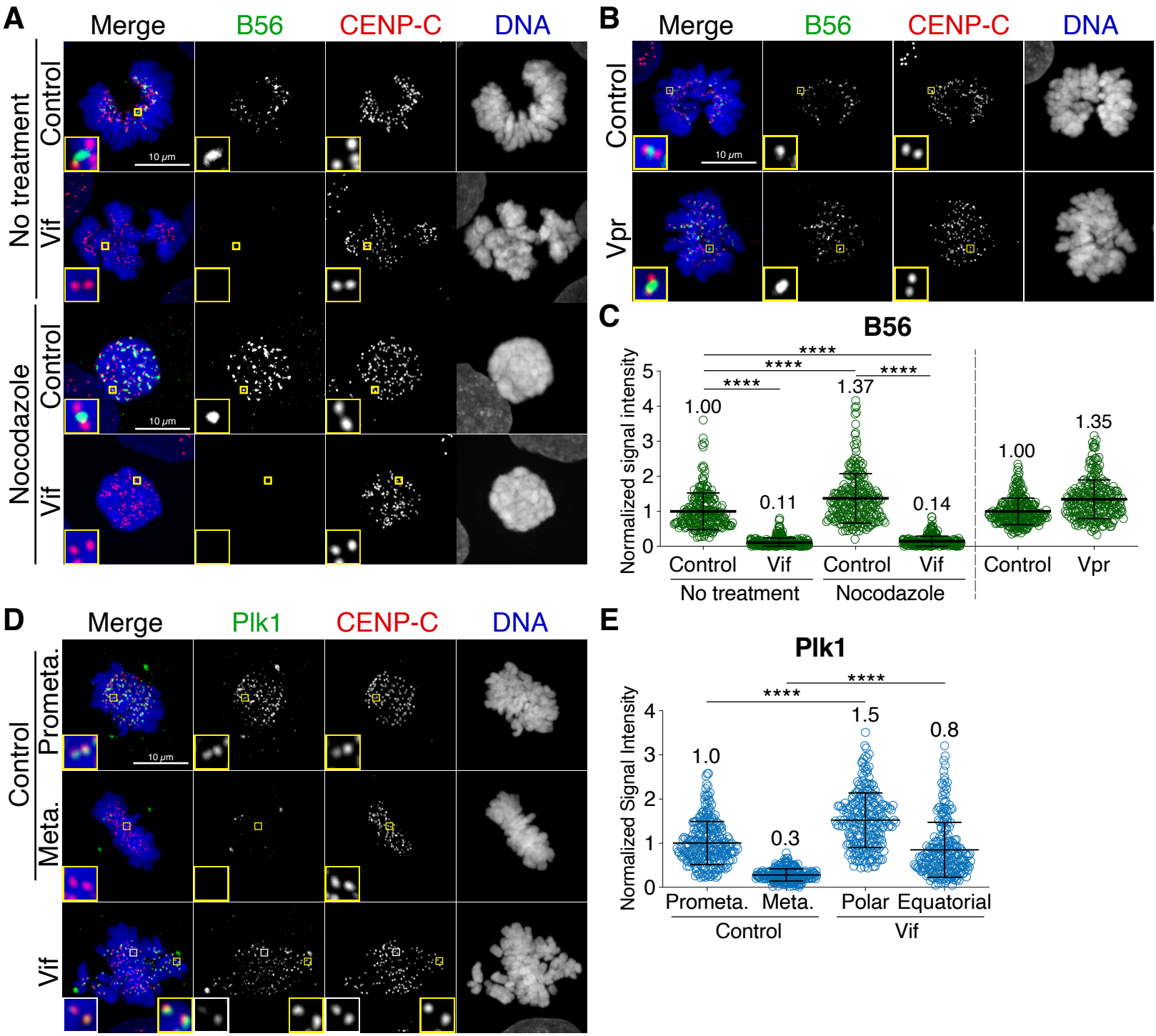
A
Merge
B56
CENP-C
DNA
No treatment
Control
Vif
Nocodazole
Control
Vif
10 μm
B
Merge
B56
CENP-C
DNA
Control
Vpr
10 μm
C
B56
Normalized signal intensity
****
****
****
****
1.00
0.11
1.37
0.14
1.00
1.35
Control
Vif
Control
Vif
Control
Vpr
No treatment
Nocodazole
D
Merge
Plk1
CENP-C
DNA
Control
Prometa.
Meta.
Vif
10 μm
E
Plk1
Normalized Signal Intensity
****
****
1.0
0.3
1.5
0.8
Prometa.
Meta.
Polar
Equatorial
Control
Vif

Figure 5

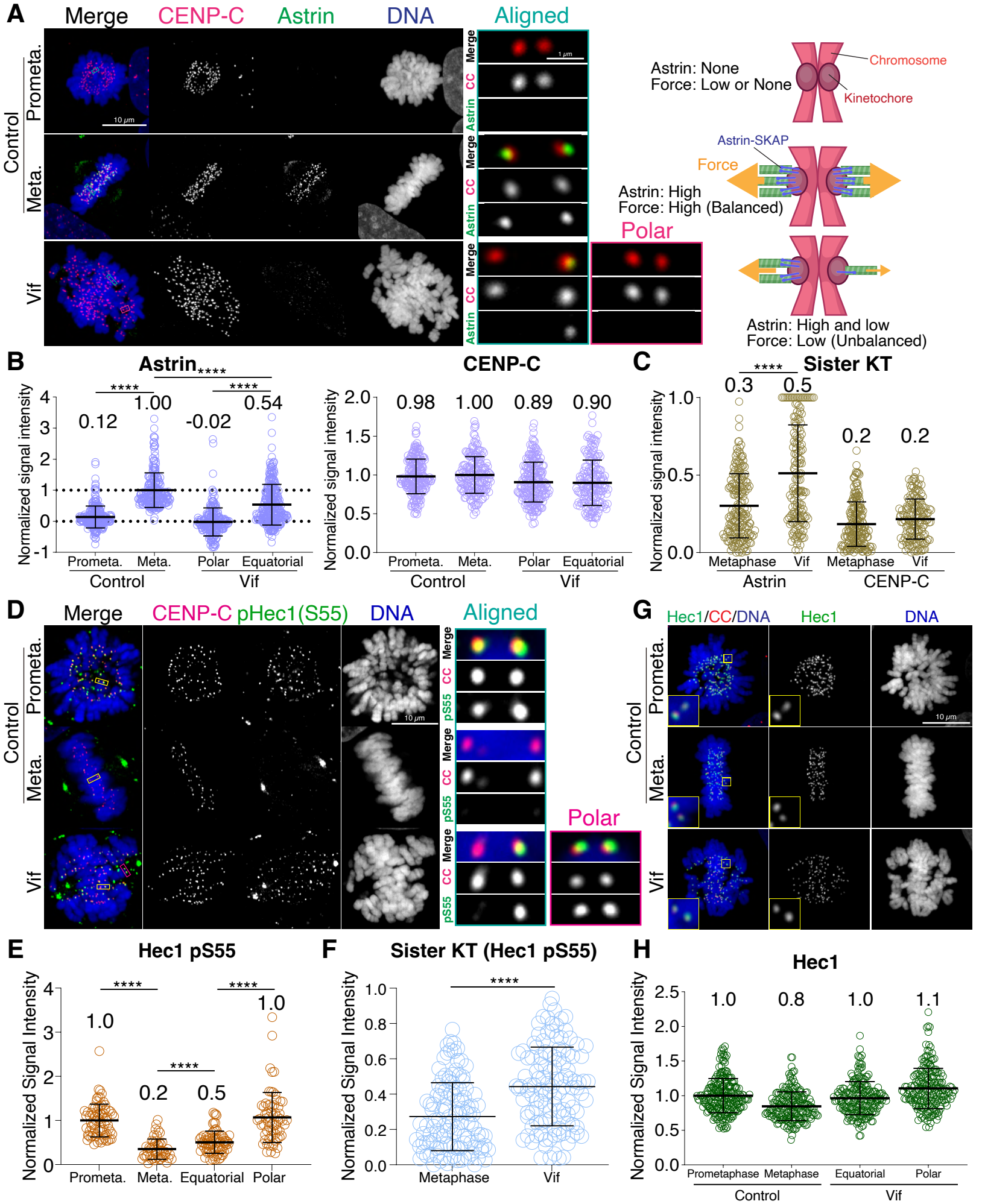
A
Merge
CENP-C
Astrin
DNA
Aligned
Control
Prometa.
Meta.
Vif
10 μm
1 μm
Merge
CC
Astrin
Polar
Astrin: None
Force: Low or None
Chromosome
Kinetochore
Astrin-SKAP
Force
Astrin: High
Force: High (Balanced)
Astrin: High and low
Force: Low (Unbalanced)
B
Astrin****
Normalized signal intensity
0.12
1.00
-0.02
0.54
Prometa.
Meta.
Polar
Equatorial
Control
Vif
CENP-C
0.98
1.00
0.89
0.90
C
Sister KT
0.3
0.5
0.2
0.2
Metaphase
Astrin
CENP-C
D
pHec1(S55)
pS55
G
Hec1/CC/DNA
Hec1
E
Hec1 pS55
Normalized Signal Intensity
1.0
0.2
0.5
1.0
F
Sister KT (Hec1 pS55)
H
Hec1
1.0
0.8
1.0
1.1
Prometaphase

Figure 6

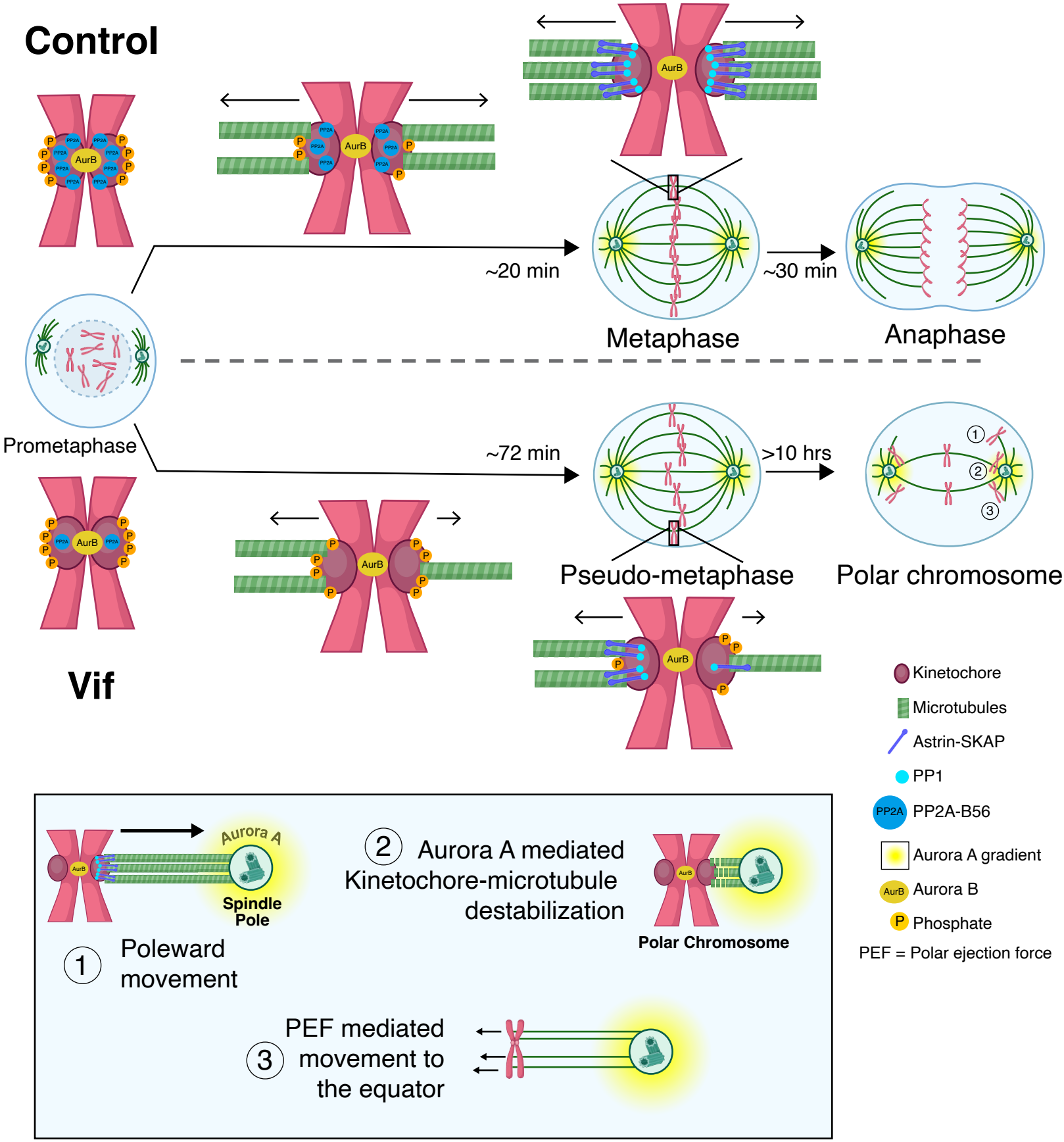
Control
AurB
PP2A
P
~20 min
~30 min
Metaphase
Anaphase
Prometaphase
~72 min
>10 hrs
Pseudo-metaphase
Polar chromosome
1
2
3
Vif
Kinetochore
Microtubules
Astrin-SKAP
PP1
PP2A-B56
Aurora A gradient
Aurora B
Phosphate
PEF = Polar ejection force
Aurora A
Spindle Pole
1 Poleward movement
2 Aurora A mediated Kinetochore-microtubule destabilization
Polar Chromosome
3 PEF mediated movement to the equator

Figure 7